JOURNAL OF SOLID STATE CHEMISTRY **129,** 250–256 (1997)
ARTICLE NO. SC967225

$Ln_3Cu_4P_4O_2$: A New Lanthanide Transition Metal Pnictide Oxide Structure Type

R. J. Cava,* H. W. Zandbergen,† J. J. Krajewski,* T. Siegrist,* H. Y. Hwang,* and B. Batlogg*

*Bell Laboratories, Lucent Technologies, Murray Hill, New Jersey 07974; and
†National Centre for High Resolution Electron Microscopy, Technical University, Delft, Holland

Received May 28, 1996; in revised form November 13, 1996; accepted November 14, 1996

A new type of lanthanide transition metal pnictide oxide, $Ln_3Cu_4P_4O_2$ (for Ln = La, Ce, and Nd), is reported. The crystal structure is made from Ln_2O_2 layers of the Pb_2O_2 type stacked with layers of Cu_2P_2 tetrahedra and indicates the existence of a homologous series of compounds with similar chemistry connecting the BiCuOSe and $ThCr_2Si_2$ structure types. The resistivity of $La_3Cu_4P_4O_2$ is metallic, with no superconductivity observed above 2 K. The Ce and Nd compounds have magnetic susceptibilities characteristic of the trivalent Lanthanides. No magnetic ordering is observed above 4.2 K. © 1997 Academic Press

INTRODUCTION

Layered transition metal oxides continue to be the source of interesting and surprising physical phenomena. The same holds true for chemically layered intermetallic compounds. There is a very small class of layered materials which represent a combination of these distinct structural chemistries: the transition metal pnictide or chalcogenide oxides (see, for instance, Refs. (1) and (2)). These materials combine commonly found layered metal–oxide structural components and layered metal–pnictide or metal–chalcogenide structural components in a surprising manner. Pnictogen, chalcogen, and oxygen all act as anions: e.g., no phosphate or selenate is formed. We began an exploration of copper oxide based pnictide oxides in the hope of finding a cuprate analog to $Ba_2Mn_3P_2O_2$, in which square planes of both Mn_2P_2 and MnO_2 are found (3). Although a lanthanide copper pnictide oxide does exist, its crystal structure does not contain CuO_2 sheets, but rather Cu_2P_2 sheets only. These are stacked with Ln_2O_2 sheets with the Pb_2O_2 structure, as are, for example, found in Nd_2CuO_4 (4). The synthesis, crystal structure, relation to known structure types, and some basic physical properties of these compounds are described in this report.

SYNTHESIS

Synthesis of the compounds in powder form in purities greater than 90% required multiple heating and grinding steps and the selection of particular starting materials. The most satisfactory starting materials were found to be fresh lanthanide metal shavings, lump red phosphorus, and Cu_2O (source of O and Cu). Using Ln_2O_3, for example, as a source of oxygen was not found to result in purities greater than approximately 75%. In addition, small amounts of excess P were added to the initial mixtures, which were of the form $Ln_3Cu_4P_{4+x}O_2$ ($x = 0.05$, 0.10, and 0.15) (approximately 1–3% excess). Best results were consistently found for the lanthanides La, Ce, and Nd for $x = 0.05$ and 0.10, where polycrystalline samples of greater than 95% purity (by powder X-ray diffraction) could be obtained. Attempts to synthesize the phase with the smaller rare earths Y, Gd, and Ho were not successful by the same method, suggesting that the phase is stable only for the larger rare earths. The powders, in 1 g quantities, were placed in dense Al_2O_3 crucibles and sealed in evacuated quartz tubes. The heating schedule was designed to accommodate high elemental P vapor pressures, low melting point intermediary phases, and a final high temperature reaction, as follows: 450°C, 550°C, 650°C, 1 day soaks; 700°C, 750°C, 800°C, 3 day soaks; grind; 850°C, 900°C, 1 day soaks; grind; 950°C, 1000°C, 1 day soaks; grind; 1050°C, 2 day soak; grind; 1050°C, 8 day soak.

STRUCTURAL CHARACTERIZATION

The new compound was discovered in an electron microscope equipped with elemental microanalysis in one of a set of exploratory synthesis. The crystallographic unit cell was determined by electron diffraction to be I centered tetragonal with approximate dimensions 0.405×2.68 nm. A more complete electron microscopy study was then performed. Electron transparent areas of the specimens were

0022-4596/97 $25.00

obtained by crushing under dry isopropanol, mounting the crushed particles on a carbon-coated holey film and then transferring into the electron microscope as quickly as possible. Electron microscopy was performed with a Philips CM30ST electron microscope with a field emission gun and Link EDX equipment operated at 300 kV. The high resolution images for the through focus exit wave reconstruction were recorded using a Tietz software package and a 1024×1024 pixel Photometric CCD camera having a dynamic range of 12 bits. The reconstructions were done using 15–20 images (with focus increments of 5.2 nm).

The exit wave reconstruction was performed with a software program developed by Coene *et al.* (5), using spherical aberation of the objective lens 1.35 mm and a defocus step of 5.2 nm. The absolute focus was determined using a maximum entropy method (6). The exit wave is displayed such that a positive phase shift and a decrease in the amplitude correspond to a darkening. Thus, for small thicknesses, the heavy scattering atoms appear as dark dots in the amplitude as well as in the phase image, allowing easy comparison of these two images.

HREM on crystals in [100] and [110] orientation clearly revealed the layers of Lanthanide and copper atoms, and on consideration of alternative models for the light atom positions, a stacking sequence of La layers, La_2O_2 layers, and Cu_2P_2 layers was found to be consistent with the experimental exit waves (see Fig. 1), indicating an overall stoichiometry of $La_3Cu_4P_4O_2$. We note that there is a significant difference in the contrast for the La atoms in the single La layer in the experimental and calculated exit waves. This indicates that the scattering potential at these columns in the experimental image is less than that at the La columns in the La–O_2–La triple layer. This difference is due to a local variation in the crystal thickness, which is related to amorphization of the crystal surface due to reaction with air (oxidation). The area at the single La layer is more susceptible to amorphization than the La–O_2–La triple layer, as can be seen from Fig. 2. Thus, given a certain

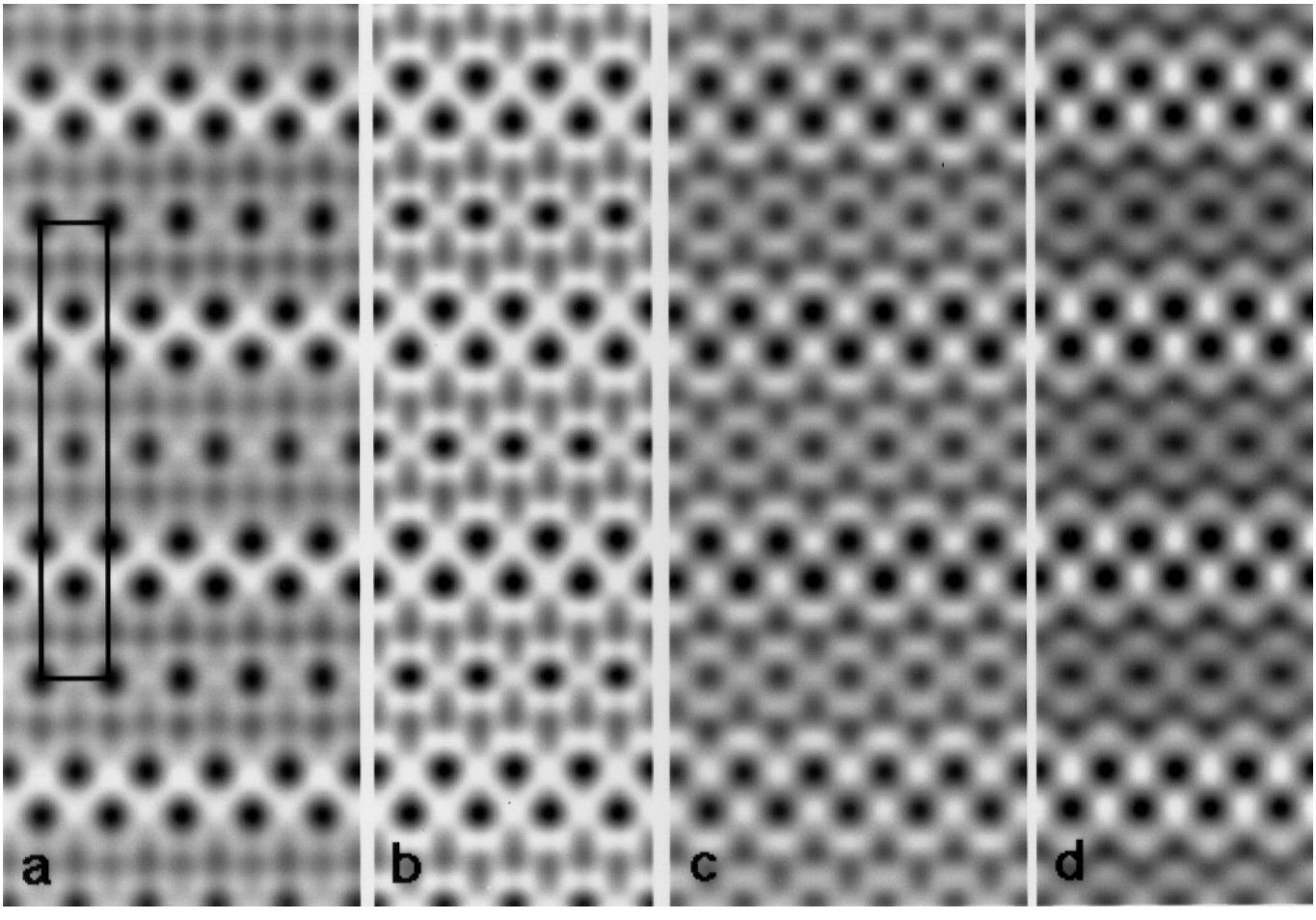

FIG. 1. Experimental exit wave image ((a) phase and (c) amplitude) of $La_3Cu_4P_4O_2$ after averaging over 4 unit cells in horizontal direction and over the mirror planes of the space group. (b) and (d) show the calculated exit wave for a thickness of 2 nm with atom positions as given in Table 2, with Debye Waller factors of 2, 1, 3, and 4 for La, Cu, P, and O, respectively, and a defocus spread to 9 nm to account for the information limit of about 0.14 nm.

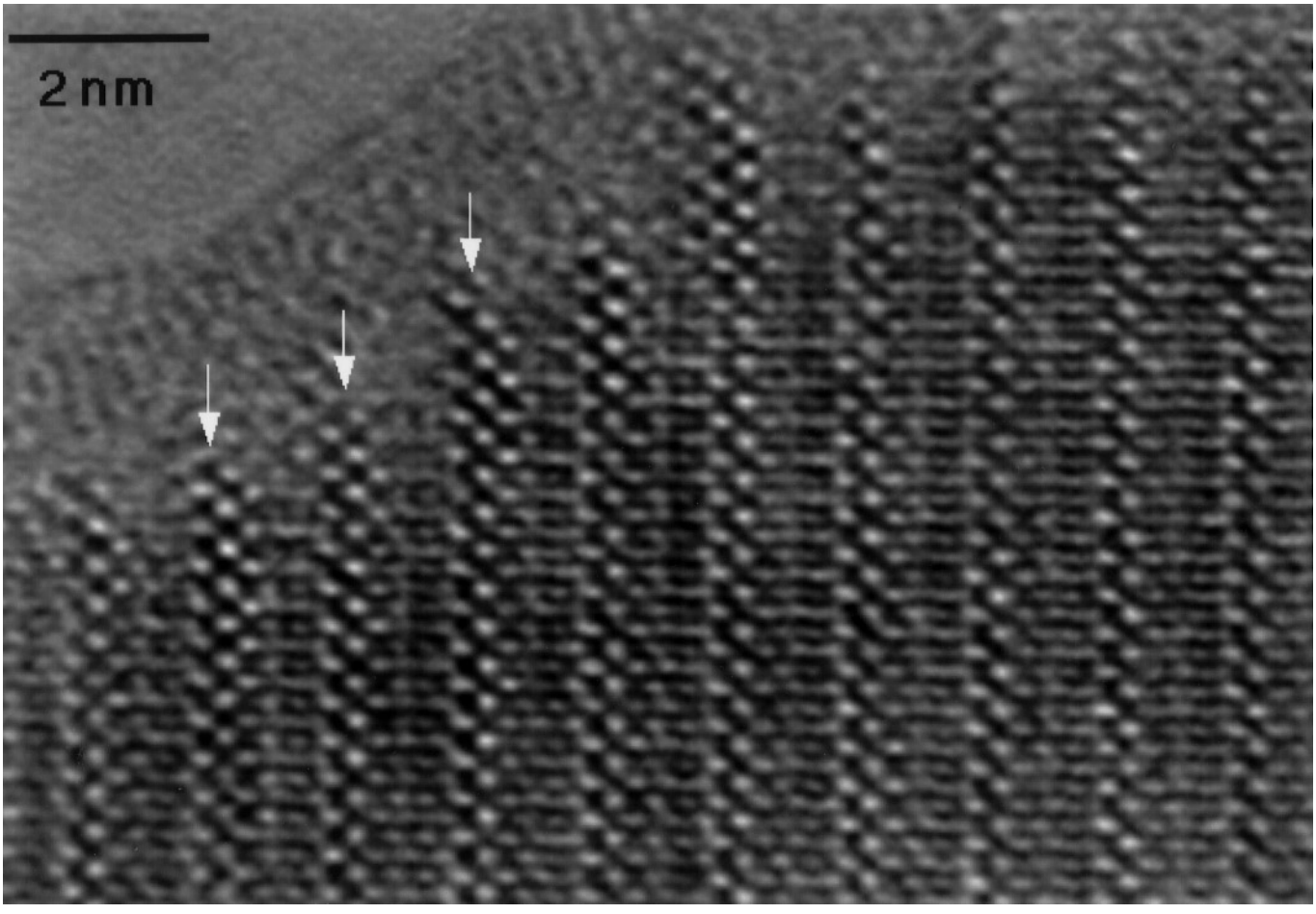

FIG. 2. Experimental HREM image of $La_3Cu_4P_4O_2$, taken at a defocus of about -80 nm, showing the further extension of the double La layers (some indicated by arrows) in the amorphous surface layer.

thickness of the crystal obtained by crushing, the remaining crystalline part is less for the area of the single La layer. This phenomenon, in which the thinner the crystal is the more eminent, can be observed in the exit wave of the edge, showing the amorphous layer extending further into the crystal at the single La layers.

A small single crystal ($0.05 \times 0.05 \times 0.07$ mm) of $La_3Cu_4P_4O_2$ was obtained from grain growth in a polycrystalline pellet of that stoichiometry heated at 1100°C. Data were collected on an Enraf-Nonius CAD-4 diffractometer with Mo$K\alpha$ radiation. Experimental conditions are described in Table 1. To correct for absorption, a psi-scan followed by spherical absorption correction was employed. The structure was refined with the NRCVAX suite of programs. The refined crystal structure atomic coordinates are presented in Table 2. The coordinates are consistent with the structure observed in the HREM study. The powder diffraction patterns of $Ce_3Cu_4P_4O_2$ and $Nd_3Cu_4P_4O_2$ were employed to obtain crystallographic cell parameters of $a = 3.985(1)$, $c = 26.573(9)$ and $a = 3.964(1)$, $c = 26.551(5)$ Å, respectively, for those compounds. Unlike the case for the quaternary layered boro-carbides (7), for the present materials (in the La case $a = 4.033(1)$, $c = 26.765(8)$), all cell parameters decrease with decreasing rare earth size.

The crystal structure of $La_3Cu_4P_4O_2$ is shown in Fig. 3. The figure shows the manner in which the La–O_2–La layers with the Pb_2O_2-type structure are stacked with the P–Cu_2–P–La–P–Cu_2–P layers with the $ThCr_2Si_2$-type structure to build up the full crystal structure. The Cu_2P_2 layers have copper in tetrahedral coordination with phosphorous. The coppers form a square planar net. The oxide and pnictide layers are joined by bonding between the La in the La_2O_2 layer and the outer P in the Cu_2P_2 layer. This results in an interesting square antiprismatic coordination for that La atom: to all O in a small square on one side and all P in a larger square on the opposing side, in a PbFCl-type arrangement. The compatibility of the sizes of the different layers is due to the fact that $d(\text{Cu–P}) \approx d(\text{La–O}) \sim d(\text{La–P})/\sqrt{2}$ allowing the layers to stack without excessive strain. Table 3 summarizes some of the near-neighbor

TABLE 1
Crystallographic Data for $La_3Cu_4P_4O_2$

Formula	$La_3Cu_4P_4O_2$
Space group	*I*4/*mmm*
Crystal size (mm)	$0.05 \times 0.05 \times 0.07$
a(Å) (at 23°C)	4.033(1)
c(Å)	26.765(8)
V (Å^3)	435.3(2)
Z	2
D_c (g/cm^3)	6.352
μ (Mo$K\alpha$, cm^{-1})	247.5
Minimum transmission	0.362
Maximum transmission	0.577
Scan type	ω
Reflections measured	2391
Independent reflections	240
Observed reflections ($I > 2.5\sigma(I)$)	149
Refined parameters	12
R	0.057
R_w ($w = 1/\sigma^2(F_0)$)	0.029
Extinction length (μm)	0.048(35)

TABLE 3
Interatomic Distances in $La_3Cu_4P_4O_2$

I. La1 (in the $LaCu_2P_2$ layer)		
La1–P2	3.062(4)	8×
–Cu	3.226(3)	8×
–P1	3.76(1)	4×
II. La2 (in the La_2O_2 layer)		
La2–O	2.397(2)	4×
–Cu	3.513(4)	4×
–P1	3.287(6)	4×
III. Cu (in the Cu_2P_2 layer)		
Cu–P1	2.369(6)	2×
–P2	2.456(7)	2×
–Cu	2.852(1)	4×
P2–Cu–P2	110.4(4)°	1×
P1–Cu–P1	116.7(4)°	1×
P1–Cu–P2	107.4(2)°	4×
IV. P2 (the P–P bondlength across the La layer in the $LaCu_2P_2$ layer)		
P2–P2	2.23(3)	1×

atomic distances and bond angles. It shows that the CuP_4 tetrahedron is slightly distorted in bond length: the P–Cu–P bond angles are 117°(1×), 110°(1×), and 107°(4×), arranged in a manner showing that the tetrahedra are flattened along the stacking direction (*c*). The table also shows that the La–O bond lengths in the La_2O_2 layer, 2.40 Å, are shorter than are usually found for La–O in perovskite related compounds (~2.7 Å) where it is not usually found in this kind of layer (4), but are similar to those commonly found for smaller rare earths in layers of this geometry. Finally, the P–P bond length across the La layer in the $LaCu_2P_2$ sandwich, 2.23 Å, is rather short. It is close to that found in elemental phosphorus (~2.25 Å) and shorter than that found for P–P bonds in Ni–P (~2.4 Å) (8). This indicates that the P in the current compound cannot be thought of as being the P^{3-} anion, acting more like $(P_2)^{4-}$.

TABLE 2
Atomic Parameters *x*, *y*, *z* and B_{iso}

	x	*y*	*z*	B_{iso}[a]
La 1	0	0	0	0.43(8)
La 2	1/2	1/2	0.20156(10)	0.90(7)
Cu	1/2	0	0.09406(12)	0.87(7)
P 1	0	0	0.1405(4)	0.32(19)
P 2	1/2	1/2	0.0417(5)	0.55(20)
O	1/2	0	1/4	3.3(9)

Note. e.s.d.s refer to the last digit printed.
[a] B_{iso} is the mean of the principal axes of the thermal ellipsoid.

COMPARISON TO OTHER STRUCTURES

Although the number of known pnictide oxides remains small, some interesting comparisons among their crystal structures can be made. Figure 4 shows, in a schematic manner, the relation between $La_3Cu_4P_4O_2$ and two previously described pnictide oxide structure types, $Ba_2Mn_3P_2O_2$ (3) and $U_2Cu_2As_3O$ (9). It can be seen that although their formulas appear at first sight to be similar, $Ba_2Mn_3P_3O_2$ and $La_3Cu_4P_4O_2$ are really rather dissimilar, with the oxygen being in a perovskite-like TO_2 layer in the former and in a Pb_2O_2-like A_2O_2 layer in the latter (where *T* is the transition metal, and *A* is the large atom such as the lanthanoid or actinioid). $U_2Cu_2As_3O$ is perhaps more closely related to $La_3Cu_4P_4O_2$, but has no single large atom layer (e.g., La); rather, it has an U_2As_2 layer with the same fluorite-like type of geometry as is found in the U_2O_2 layer. The similarity in chemistry of these two structure types suggests that phases might be found which are a hybrid between the two.

Consideration of the crystal structure of $La_3Cu_4P_4O_2$ in the context of other known compounds (9–13) suggests the existence of a homologous series between those of the relatively rare BiCuOSe structure type and those of the ubiquitous $ThCr_2Si_2$ intermetallic structure type. The homologous series is illustrated schematically in Fig. 5, where the known compounds with related chemistry ThCuPO (9) and $LaNi_2P_2$ (14) are selected to represent the end-members and $Th_3Ni_3P_3O$ (9) and $La_3Cu_4P_4O_2$ as the first few members of the series. The series is generated by the stacking of "$Th_2Cu_2P_2O_2$"-type layers with "$LaNi_2P_2$"-type layers, as

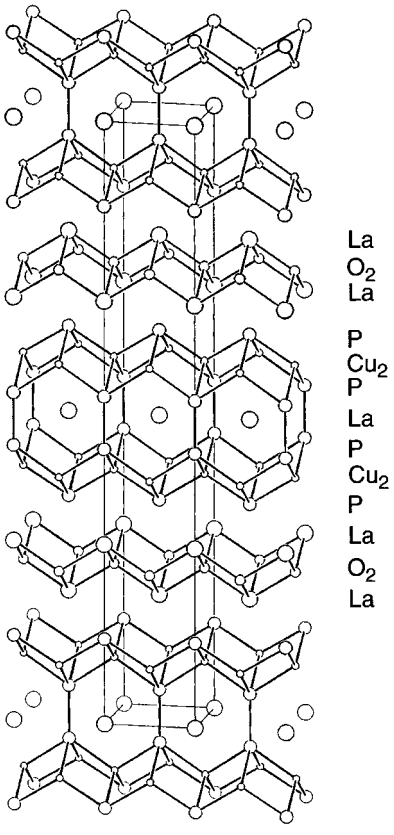

FIG. 3. The crystal structure of $La_3Cu_4P_4O_2$. Outline shows the crystallographic unit cell. The layers are identified on the side of figure: the layered nature of the crystal structure is emphasised via the interatomic bonds shown.

shown in the figure. The formula for the series is therefore

$$(A_2O_2T_2P_2)_m \cdot (AT_2P_2)_n.$$

Members of the series have been observed for $m = 1$ and $n = 0, 1, 2,$ and ∞, as shown in the figure. To our knowledge, no examples are known for $m \neq 1$ or n larger than 2 and less than ∞. This relationship between the relatively rare pnictide oxides and the common $ThCr_2Si_2$ structure type suggests that the potential exists for the discovery of many new materials with related chemistry and structure.

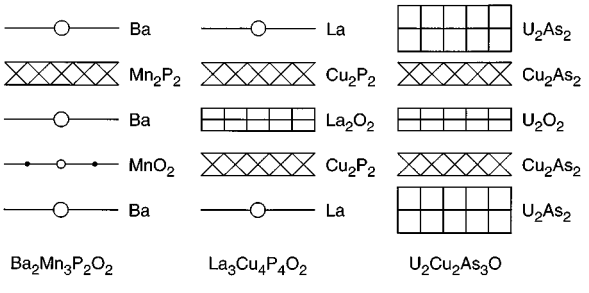

FIG. 4. Schematic comparison of the structure types of 3 known layered transition metal pnictide oxides. Each has a 4 layer stacking repeat. The 5 types of elementary layers are shown: A, A_2O_2, A_2X_2, and T_2X_2, and TO_2; where A is the large ion, T the transition metal, X the pnictogen, and O oxygen.

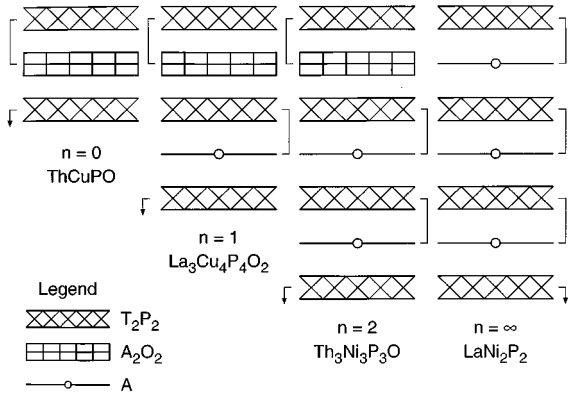

FIG. 5. Schematic comparison of the crystal structures of known members of the new homologous series $(A_2O_2T_2X_2)_m(AT_2X_2)_n$ for $m = 1$ and n as shown, and A, T, X, and O defined as in Fig. 4.

PHYSICAL PROPERTIES

The electrical resistivity of a $La_3Cu_4P_4O_2$ polycrystalline pellet was measured between 300 and 4.2 K in a standard 4-probe geometry. The behavior of $\rho(T)$ is shown in Fig. 6. The room temperature resistivity is 250 μ ohm cm, and the resistivity at 4 K 30 μ ohm cm, showing this material to be

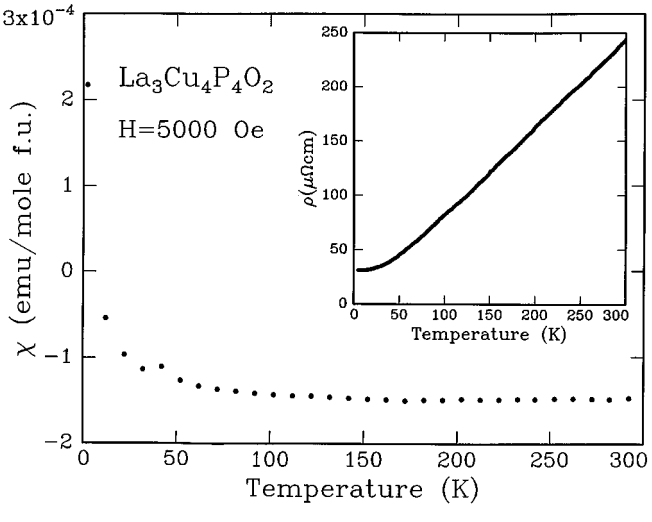

FIG. 6. Magnetic susceptibility of $La_3Cu_4P_4O_2$ measured in a 5 kOe field. Inset: Temperature dependent resistivity of a polycrystalline sample of $La_3Cu_4P_4O_2$.

a good metal even in polycrystalline form where there may be a significant contribution from grain boundary resistivity. The inset to Fig. 6 shows the variation of magnetic susceptibility between 300 and 4 K measured in a field of 5000 Oe (SQUID magnetometer). The susceptibility is basically diamagnetic and temperature independent, dominated by core diamagnetism and only a weak Pauli paramagnetism from the conduction electrons. A very small contribution from uncompensated Cu^{2+} spins is observed at low temperature, possibly from impurity phases, at the level of 0.4%. The magnetic susceptibility of $Nd_3Cu_4P_4O_2$ is shown in Fig. 7 as $1/\chi$ vs T, showing the Curie–Weiss behavior at high temperature with a deviation at low temperature. A fit to the high temperature data indicates a moment of 3.68 μ_B/Nd, comparing favorably to the expected moment of 3.62 μ_B/Nd. The Curie–Weiss θ from the fit is 23.0 K, indicating antiferromagnetic correlations between the Nd spins. However, no magnetic ordering is observed above 4.2 K indicating at least a moderate degree of frustration of the Nd spins.

The magnetic susceptibility of $Ce_3Cu_4P_4O_2$ is presented in Fig. 8. In this case, curvature is seen for the entire temperature range between 4 and 300 K. Again, no signature of magnetic ordering is observed. The Ce moment obtained from the high temperature data is 2.33 μ_B/Ce (with a θ of 39.2 K), slightly reduced from the expected value of 2.54 μ_B/Ce. The temperature dependence of $1/\chi$ vs T deviates from Curie–Weiss significantly at low temperatures due to crystal field effects, which depopulate the excited $4f$ states with decreasing temperature and decrease the apparent moment. The temperature dependent resistivity of a polycrystalline sample of $Ce_3Cu_4P_4O_2$ is shown in Fig. 9. The resistivity is higher than that of $La_3Cu_4P_4O_2$, due to scattering of the charge carriers by the Ce moments. The knee in the resistivity near 150 K is due to the decreased carrier scattering as the excited states for Ce are depopulated with decreasing temperature.

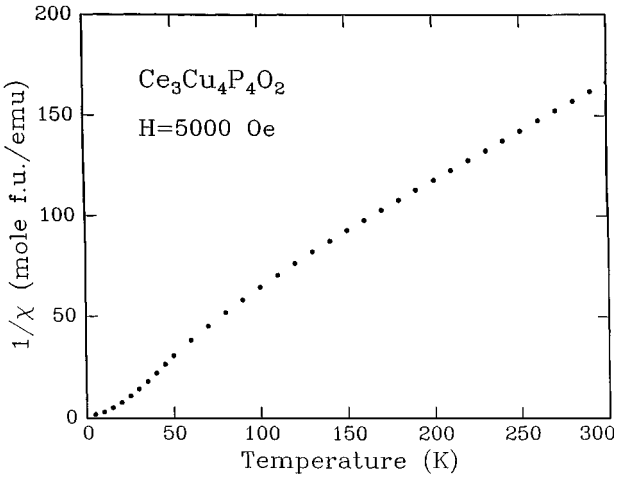

FIG. 8. Magnetic susceptibility of $Ce_3Cu_4P_4O_2$ in 5 kOe as $1/\chi$ vs T.

CONCLUSIONS

The synthesis, crystal structure, and basic physical properties of a few members of a new layered transition metal pnictide oxide structure type of stoichiometry $Ln_3Cu_4P_4O_2$ have been described. Comparison with other known transition metal pnictide oxides suggests the possibility that this so far rather limited class of materials has the potential for discovery of a considerably larger number of members with a variety of related crystal structures. More detailed study of the physical properties of some of these compounds would be of significant interest.

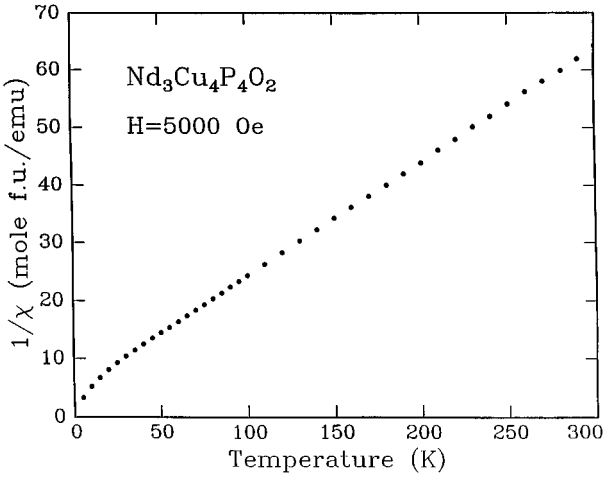

FIG. 7. Magnetic susceptibility of $Nd_3Cu_4P_4O_2$ in 5 kOe as $1/\chi$ vs T.

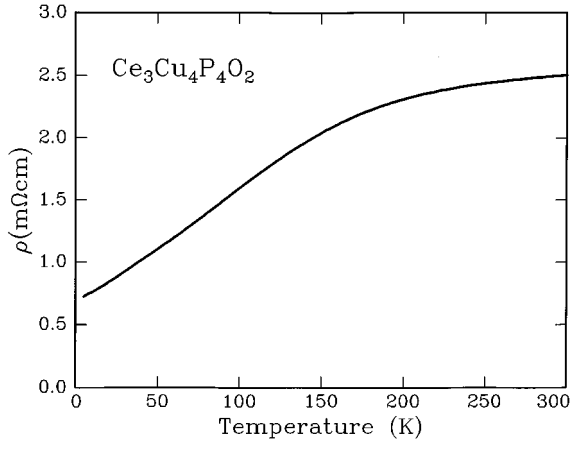

FIG. 9. The temperature dependent resistivity of a polycrystalline sample of $Ce_3Cu_4P_4O_2$.

REFERENCES

1. S. L. Brock and S. M. Kauzlarich, *Comments Inorg. Chem.* **17,** 213 (1995).
2. Y. Park, D. C. DeGroot, J. L. Schindler, C. R. Kannewurf, and M. G. Kanatzidis, *Chem. Mater.* **5,** 8 (1993).
3. Ned T. Stetson and Susan M. Kauzlarich, *Inorg. Chem.* **30,** 3969 (1991).
4. H. Müller-Buschbaum and W. Wollschlager, *Z. Anorg. Allg. Chem.* **414,** 76 (1975).
5. W. J. M. Coene, A. Thust, M. op de Beek, and D. Van Dyck, *Ultramicroscopy*, in press.
6. D. Tang, J. Jansen, H. W. Zandbergen, M. op de Beek, and D. Van Dyck, *Ultramicroscopy*, in press.
7. T. Siegrist, R. J. Cava, J. J. Krajewski, and W. F. Peck, Jr., *J. Alloys Comp.* **216,** 135 (1994).
8. A. F. Wells, "Structural Inorganic Chemistry," pp. 838–875. Clarendon Press, Oxford, 1984.
9. D. Kaczorowski, J. H. Albering, H. Noel, and W. Jeitschko, *J. Alloys Comp.* **216,** 117 (1994).
10. P. S. Berdonosov, A. M. Kusainova, L. N. Kholodkovskaya, V. A. Dolgikh, L. G. Akselrud, and B. A. Popovkin, *J. Solid State Chem.* **118,** 74 (1995).
11. B. I. Zimmer, W. Jeitschko, J. H. Albering, R. Glarum, and M. Reehuis, *J. Alloys Comp.* **229,** 238 (1995).
12. J. H. Albering and W. Jeitschko, *Z. Naturforsch B* **51,** 257 (1996).
13. D. Kaczorowski, J. H. Albering, and H. Noel, *J. Solid State Chem.* **112,** 228 (1994).
14. W. Jeitschko and B. Jaberg, *J. Solid State Chem.* **35,** 312 (1980).